Accepted Manuscript

Characterisation of L2$_1$-ordered Ni$_2$TiAl precipitates in Fe-Mn maraging steels

Feng Qian, Joanne Sharp, W. Mark Rainforth

The paper is entitled:

Characterisation of L2$_1$-ordered Ni$_2$TiAl precipitates in Fe-Mn maraging steels

Authors:

Feng Qian

Department of Materials Science and Engineering, University of Sheffield, Sir Robert Hadfield Building, Mappin Street, Sheffield S1 3JD, UK

Joanne Sharp

Department of Materials Science and Engineering, University of Sheffield, Sir Robert Hadfield Building, Mappin Street, Sheffield S1 3JD, UK

W Mark Rainforth (corresponding author)

Telephone: +44 (0) 114 222 5469

Fax: +44 (0) 114 222 5943

Email: m.rainforth@sheffield.ac.uk

Address: Department of Materials Science and Engineering, University of Sheffield, Sir Robert Hadfield Building, Mappin Street, Sheffield S1 3JD, UK

Abstract

The precipitates formed in a new series of Fe-Mn maraging steels when aged at 500 °C were identified as the $L2_1$-ordered Ni_2TiAl phase. The precipitate formed a coherent-coplanar microstructure analogously to γ/γ' Ni-based superalloys and maintained a high number density and homogeneous dispersion within α'-martensite matrix even after aging for 10,080 min. An increase in the Mn content of the alloy led to faster precipitation kinetics and thus rapid hardening kinetics.

Keywords: maraging steels, Ni_2TiAl, precipitation hardening, coarsening behaviour, transmission electron microscopy

1   Introduction

In response to automotive requirements for reducing production costs and lightweight strategies, the current trend in the steel industry is to develop leaner compositions with improved strength-elongation balances [1][2][3]. Recently, a group of newly-developed 9-12 wt.% Mn lean maraging TRIP (transformation induced plasticity) steels with minor additions of Ni, Ti and Mo was reported to possess an excellent combination of strength and ductility (e.g. 12 wt.% Mn alloy: ultimate tensile strength (UTS): ~1.3 GPa, total elongation (TE): ~21%) [4][5]. The authors attributed the simultaneous increase of strength and ductility upon aging to the joint effect of precipitation strengthening mechanism and TRIP mechanism of retained austenite. However, the characterisation of precipitates in these Fe-Mn maraging steels is a matter of debate. Initially, both atom probe tomography (APT) and local energy-dispersive X-ray spectroscopy (EDS) analyses revealed the precipitates were enriched in Ni, Al and Ti and it was speculated that the precipitates might be γ'-$Ni_3(Ti,Al)$ phase which is the most common precipitates in conventional 18Ni maraging steels [4][5]. However, later Millán et al. reported that the average chemical composition was closer to $Ni_{50}(Al,Ti,Mn)_{50}$

[6]. A more recent APT study proposed the formation of NiMn or/and Ni_2MnAl precipitates was dependent on the Al contents in Mn maraging steels [7]. The current work reports a detailed analysis of the precipitates correlated with the ageing kinetics.

2 Materials and Experimental methods

Based on the previous research, a further study on the precipitation behaviour in Fe-Mn maraging steels was carried out at 500 °C. This temperature was chosen as it is the conventional aging temperature for maraging steels, and our preparative work indicated that this temperature offered the best combination of time, temperature and peak hardness value. In view of the active role of Al in precipitation-strengthened steels (e.g. NiAl-strengthened steels), ~1 wt.% Al was added to the Mn maraging TRIP steels in Ref. [4]. The chemical compositions of the studied alloys are given in Table 1. The characterisation of precipitates was made based on the chemical composition and crystal structure analyses. According to the investigation on the precipitation evolution, the coarsening kinetics of precipitates was studied.

The ingots were homogenized under argon gas atmosphere at 1150 °C for 1 hour followed by hot rolling with a reduction ratio of 85% between 1140 °C and 850 °C. The subsequent solution heat treatment was performed with argon protection at 1050 °C for 0.5 h. The alloys were then aged at 500 °C for a range of times from 10 min to 10080 min. Vickers hardness measurements were conducted on aged samples with a load of 294 N (30 kg) and a dwell time of 15 s. Each result was averaged from at least eight measurements. Thin foils for transmission electron microscopy (TEM) study were prepared by a solution of 5% perchloric acid, 35% butoxyethanol and 60% methanol solution (maintained at approximately -40 °C by a liquid nitrogen cooling system) running through a twin-jet electropolisher operated at ~40

mA. In order to exclude the interference from surrounding phases, carbon extraction replicas were prepared for the TEM investigation on nano-size precipitates. Microstructural observation and elemental analyses were carried out using an FEI Tecnai at 200 kV and high resolution imaging was taken on a JEOL 2010F at 200 kV. All the crystallographic information is from International Centre for Diffraction Data (ICDD) database (card number 04-004-2487 and 00-019-0034).

3   Results and discussion

3.1   Hardness evolution

Figure 1 displays the hardness-time curves of 7%, 10% and 12% Mn alloys aged at 500 °C, which exhibit the typical hardness evolution of precipitate-strengthened alloys. Rapid hardening reaction was observed in the early aging stage of 10% and 12% Mn alloys, over 90% of the total increase in hardness was achieved within the first 30 minutes. While an incubation time for hardness increase was evident in the 7% Mn alloy, hardening then occurred rapidly to the peak hardness after around 240 minutes. Nevertheless, the maximum hardness of the three alloys was close (i.e. 7% Mn alloy: 418 HV at 240 min; 10% Mn alloy: 421 HV at 240 min; 12% Mn alloy: 432 HV at 120 min). It is worth noting that in the over-aged region, what appears to be secondary hardening is visible in both 10% and 12% Mn alloys which is associated with the formation of reverted austenite (which will be reported in detail elsewhere).

3.2   Chemical composition of precipitates

Figure 2 presents TEM micrographs of precipitates formed in 7% and 12% Mn alloys when aged at 500 °C. The 10% Mn alloy exhibited behaviour similar behaviour to the higher and lower Mn alloys. The 500 °C / 480 min state in Figure 2(a) for the 7% Mn alloy, which

corresponds to the peak hardness condition, exhibits well dispersed fine precipitates ($\bar{r} = 2.52 \pm 0.72$ nm). Further aging for 2880 min led to a moderate increase in the size of precipitates ($\bar{r} = 5.20 \pm 1.79$ nm), as shown in Figure 2(c). Continuous precipitate coarsening was observed with a decrease in the number density (measured from extraction replicas) evident in the 10,080 min aged samples (Figure 2(e)). Similarly in the 10% Mn (not shown here because the tendency was the same as in other two alloys) and 12% Mn alloy, further aging up to 10080 min resulted in a significant increase in the precipitate size and a decrease in the number density (Figure 2(d) and (f)).

Local TEM-EDS analysis was performed on thin foil samples and representative spectra of both the matrix and precipitates (7 % Mn, 500 °C / 10080 min) are presented in Figure 3(a). The spectrum of precipitate indicates that the precipitate contained Ni, Ti and Al when compared to the surrounding matrix. The major elements of the martensite matrix, Fe and Mn, were also detected in precipitates. Some researchers suggested that the Fe and Mn concentrations were due to the residual matrix above or below precipitates [8], but in this study the Mn/Fe atomic ratio of precipitate (72.4%) is much higher than that of the matrix (7.4%).

In order to minimize the interference from the matrix, carbon extraction replicas were studied by TEM. TEM-EDS analyses on replica samples (Figure 3(b)) confirms that the precipitates mainly comprised Ni, Ti and Al with a small amount of Fe and Mn substitution (Fe: ~12 at.%; Mn: ~5 at.%). APT analysis by Millán et al. [6] also confirmed the existence of Fe and Mn in precipitates and 20 at.% Fe and 24 at.% Mn were detected in precipitates in a 9% Mn alloy aged at 450 °C for 192 h. Similar phenomenon has been reported in several NiAl-strengthened steels [9][10][11][12][13] and it is suggested that NiAl precipitates which are

formed out of the solute-rich clusters have a high solubility of Fe. On the other hand, the well-known Ni_3Ti precipitates in conventional 18Ni maraging steels are generally Fe-free [12][14][15]. Therefore, the presence of Fe atoms indicates that the precipitate in this study is more likely to be NiAl phase or similar phases with high Fe solubility. Our study suggests that the chemical composition of precipitates is more likely to be non-stoichiometric Ni_2TiAl or Ni(Ti,Al), which is in contrast to the work by Raabe and his colleagues [5][7] who speculated the precipitates might be $Ni_3(Ti,Al)$ phase or $NiMn/Ni_2MnAl$ phase.

3.3 Crystal structure of precipitates

NiAl phase with a B2 structure is a common type of precipitate in Fe-Al-Ni alloys and has been extensively studied [9][13][16]. While $L2_1$-type Ni_2TiAl phase is often reported in TiNi alloys but rarely observed as precipitates in Fe-based alloys. Recently, Liebscher et al. [8] and Sun et al. [17] proposed a new design approach of precipitation-hardened ferritic alloys where $L2_1$-Ni_2TiAl or $L2_1$-Ni_2TiAl/B2-NiAl phase was generated as the dominant strengthening precipitates. Figure 4(a) and (c) display the simulated crystal structure of B2-NiAl phase and electron diffraction pattern along [011] zone axis, respectively. The B2 phase has a CsCl-type crystal structure which can be described as a body centred cubic (bcc) lattice of Ni with the centre positions being replaced by Al atoms. The lattice parameter of the stoichiometric composition is 0.2887 nm which is very close to that of α'-martensite ($Fe_{83.5}Mn_{16.5}$, 0.2884 nm). The $L2_1$-Ni_2TiAl phase simply involves a further ordering of Al and Ti atoms on the Al sublattice in B2-NiAl phase. The unit cell is built up by eight small bcc lattices. The vertices of each small cubic lattice are occupied by Ni atoms with the centre positions being orderly occupied by Al and Ti atoms. Thus, two different types of B2 structure are arranged successively in each direction. The average lattice parameter of the small bcc lattice (half that of the entire unit cell) is 0.295 nm which is close to that of B2-NiAl phase and α'-martensite. When the Al and Ti atoms are randomly arranged, the phase is

degraded to B2-ordered Ni(Al,Ti) phase; when the centre positions are fully occupied by one type of atoms, e.g. Al, the phase is transformed to B2-ordered NiAl phase.

High resolution electron microscopy (HREM) study was carried out to identify the crystal structure of precipitate. Figure 5 shows HREM micrographs of precipitate along the [011] and [$\bar{1}$11] zone axis with fast Fourer transform (FFT) analyses displayed as inset. The characteristic {111} reflections along the [011] zone axis of L2$_1$-ordered structure are indexed (see inset in Figure 5(a)). As shown in Figure 5(b) and (d), the atomic arrangement of precipitate is perfectly coincident with that of Ni$_2$TiAl phase. The indexed d-spacing of 0.3335 nm for the {111} planes and 0.206 nm for the {220} planes are very close to the standard d-spacing of Ni$_2$TiAl phase (0.3377 nm for {111} planes and 0.2068 nm for {220} planes) given by ICCD database.

3.4   Orientation relationship between the martensite matrix and precipitates

More information about the crystal structure and the orientation relationship of precipitates was obtained by selected area election diffraction (SAED) as shown in Figure 6. The presence of the {11$\bar{1}$} superlattice spots unique to the L2$_1$ structure (see inset of Figure 6(a)) further confirms the precipitate is L2$_1$-ordered Ni$_2$TiAl phase. The SADPs reveal that the orientation of the L2$_1$-ordered Ni$_2$TiAl precipitates is consistent with that of the α'-martensite matrix (see Figure 6). Moreover, in the [011] and [001] zone axis (inset of Figure 6(a) and Figure 6(b)), the {040} and {220} reflections of L2$_1$-Ni$_2$TiAl phase are overlapping with the {020} and {110} reflections of the martensite matrix, respectively; in the [$\bar{1}$11] zone axis, the diffraction pattern of Ni$_2$TiAl exactly matches that of the matrix, therefore no extra diffraction spot originating from the precipitates is observed (Figure 6(c)). This cubic-on-cubic (CoC) orientation relationship between precipitates and matrix has been reported in

several other alloys. The classical group is γ/γ' Ni-based superalloys in which the fcc Ni matrix is strengthened by the coherent L1$_2$-ordered precipitates [18]. Analogously in Fe-based alloys, B2-ordered NiAl phase is known to have a similar crystal structure to α-Fe matrix [17].

The lattice parameter of L2$_1$-ordered Ni$_2$TiAl phase was determined according to the SAED. The camera length was calibrated using the lattice parameter of α'-martensite matrix measured from XRD analysis. Based on the calibration, the lattice parameter of L2$_1$-ordered Ni$_2$TiAl phase was calculated as 0.5819 nm (based on the precipitates in the 12% Mn alloy aged at 500 °C for 2880 min). Half of the lattice parameter of L2$_1$-ordered Ni$_2$TiAl, which is the dimension of the small bcc lattice in Figure 4(b), is close to the lattice parameter of α'-martensite matrix (a = 0.2874 nm). The misfit between them is calculated as:

$$\delta = \frac{2 \times |\frac{1}{2} a_{Ni_2TiAl} - a_{bcc}|}{\frac{1}{2} a_{Ni_2TiAl} + a_{bcc}} \times 100\% = 1.24\% \tag{1}$$

Based on the small lattice misfit and the special orientation relationship between the two phases, it is proposed that the L2$_1$-ordered Ni$_2$TiAl precipitate is not only coherent but also coplanar with α'-martensite matrix. Figure 7 presents the uniformly dispersed precipitates within the matrix in 7% and 10% Mn alloys. According to Ashby-Brown contrast theory [19], the classic dumb-bell dynamical diffraction contrast from the precipitates under two-beam conditions indicates that they remained coherent with the matrix even after aging for 10080 min.

3.5 Coarsening behaviour of precipitates

Precipitate coarsening behaviour in 7%, 10% and 12% Mn alloys when aged at 500 °C are shown by plotting cube of mean precipitate radius $\bar{r}^3$ as a function of aging time t in Figure 8. Except the 500 °C / 10080 min state of 12% Mn alloy, the linear slopes in Figure 8 reveal that the relationship between the mean precipitate radius and aging time follows the Equation:

$$\bar{r}^3 - r_0^3 = K(t - t_0) \tag{2}$$

where K is the coarsening rate constant, t_0 is any time at or after the initiation of coarsening, r_0 is the precipitate radius at t_0. It suggests that the coarsening kinetics of precipitates in the three alloys is consistent with the diffusion-controlled coarsening kinetics predicted by Lifshitz-Slyozov-Wagner (LSW) theory [20][21]. The $\bar{r}^3$ of 12% Mn alloy at the 500 °C / 10,080 min state which shows a deviation from the value predicted by LSW model indicates a change in coarsening mechanism or possibly a change in precipitate structure. Further work would be required to understand this change.

As shown in Figure 8, the coarsening rate constant K increased with increased Mn content (i.e. 7% Mn alloy: 0.76×10^{-30} m^{3}s^{-1}; 10% Mn alloy: 1.48×10^{-30} m^{3}s^{-1}; 12% Mn alloy: 2.83×10^{-30} m^{3}s^{-1}). The hardness curves in Figure 1 and microstructural evolution in Figure 2Figure 2 also indicate that Mn addition effectively increased the number density and size of Ni$_2$TiAl precipitates, leading to an increase in precipitation hardening kinetics. This resulted in an increase in peak hardness with increase in Mn content. The full effect of the precipitate size and number density is considered in a separate paper which considers the correlation of microstructure with mechanical properties [22].

4 Conclusions

In summary, the elemental and crystal structure analyses demonstrated that the precipitates formed in 7-12% Mn maraging steels when aging at 500 °C were $L2_1$-ordered Ni_2TiAl phase. One-eighth of the unit cell of Ni_2TiAl precipitates coincides with the unit cell of α'-martensite matrix and the misfit between them is about 1.24%. This small misfit along with the special orientation relationship indicated that the Ni_2TiAl precipitates were not only coherent, but also coplanar with the matrix. The investigation on the coarsening behaviour and hardening effect of precipitates revealed that higher Mn content of alloy led to a faster precipitation reaction and thus a faster hardening kinetics. This study on the nature of precipitates helps to understand the precipitation strengthening behaviour of Fe-Mn maraging steels.

Acknowledgements

References:

[1]   A. Haldar, S. Suwas, D. Bhattacharjee, eds., Microstructure and Texture in Steels, Springer London, London, 2009.

[2]   S. Keeler, M. Kimchi, eds., Advanced High-Strength Steels Application Guidelines Version 5.0, WorldAutoSteel, 2014.

[3]   B.C. De Cooman, P. Gibbs, S. Lee, D.K. Matlock, Metall. Mater. Trans. A 44 (2013) 2563.

[4]   D. Raabe, D. Ponge, O. Dmitrieva, B. Sander, Adv. Eng. Mater. 11 (2009) 547.

[5]   D. Raabe, D. Ponge, O. Dmitrieva, B. Sander, Scr. Mater. 60 (2009) 1141.

[6]   J. Millán, D. Ponge, D. Raabe, P. Choi, O. Dmitrieva, Steel Res. Int. 82 (2011) 137.

[7]   J. Millán, S. Sandlöbes, A. Al-Zubi, T. Hickel, P. Choi, J. Neugebauer, D. Ponge, D. Raabe, Acta Mater. 76 (2014) 94.

[8]   C.H. Liebscher, V. Radmilovic, U. Dahmen, M. Asta, G. Ghosh, J. Mater. Sci. 48 (2013) 2067.

[9]   Z. Guo, W. Sha, D. Vaumousse, Acta Mater. 51 (2003) 101.

[10]   M. Schober, R. Schnitzer, H. Leitner, Ultramicroscopy 109 (2009) 553.

[11]   S. Höring, N. Wanderka, J. Banhart, Ultramicroscopy 109 (2009) 574.

[12]   H. Leitner, M. Schober, R. Schnitzer, Acta Mater. 58 (2010) 1261.

[13]   Z.K. Teng, C.T. Liu, G. Ghosh, P.K. Liaw, M.E. Fine, Intermetallics 18 (2010) 1437.

[14]   H. Leitner, R. Schnitzer, M. Schober, S. Zinner, Acta Mater. 59 (2011) 5012.

[15]   D.H. Ping, M. Ohnuma, Y. Hirakawa, Y. Kadoya, K. Hono, Mater. Sci. Eng. A 394 (2005) 285.

[16]   Z.K. Teng, M.K. Miller, G. Ghosh, C.T. Liu, S. Huang, K.F. Russell, M.E. Fine, P.K. Liaw, Scr. Mater. 63 (2010) 61.

[17]   Z. Sun, C.H. Liebscher, S. Huang, Z. Teng, G. Song, G. Wang, M. Asta, M. Rawlings, M.E. Fine, P.K. Liaw, Scr. Mater. 68 (2013) 384.

[18]   J.S. Van Sluytman, T.M. Pollock, Acta Mater. 60 (2012) 1771.

[19]   M.F. Ashby, L.M. Brown, Philos. Mag. 8 (1963) 1083.

[20]   I.M. Lifshitz, V.V. Slyozov, J. Phys. Chem. Solids 19 (1961) 35.

[21]   C. Wagner, Zeitschrift Für Elektrochemie, Berichte Der Bunsengesellschaft Für Phys. Chemie 65 (1961) 581.
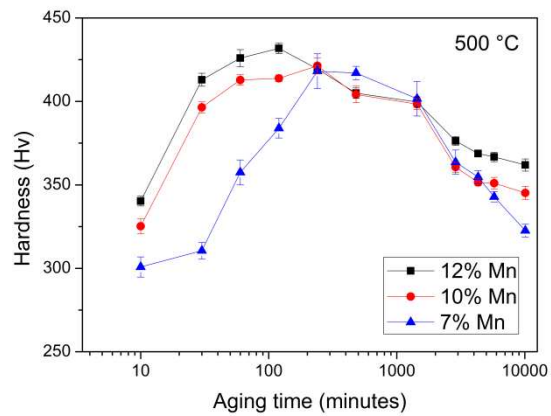
[22]   F. Qian, W. M. Rainforth, to be published.

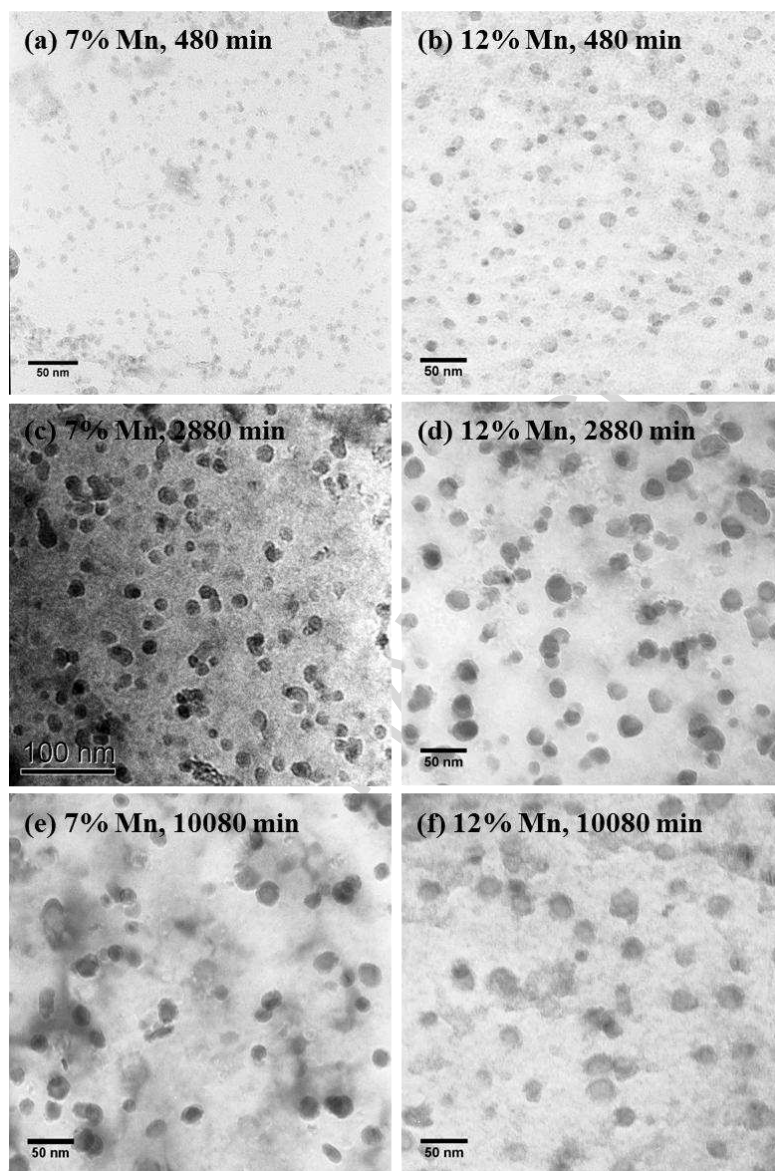Figure 1 Vickers hardness evolution of 7%, 10% and 12% Mn alloys aged at 500 °C.

Figure 2 TEM micrographs of precipitates formed at 500 °C taken. The images of 480 min state were taken on replicas owing to the ultrafine size of precipitates.
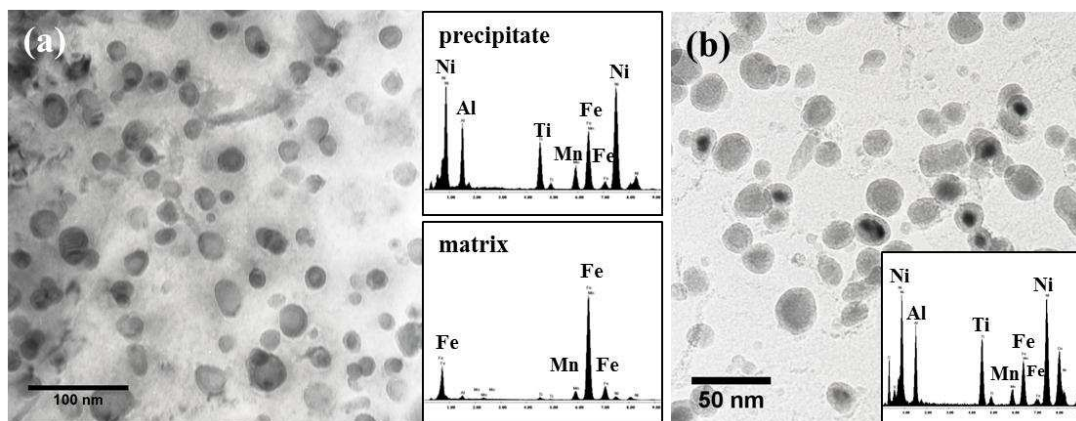
Figure 3 (a) TEM micrograph of 7% Mn alloy aged at 500 °C for 10080 min and corresponding TEM-EDS spectra of precipitate and martensite matrix; (b) TEM replica micrograph of precipitates (12% Mn, 500 °C / 2880 min) and TEM-EDS spectrum.
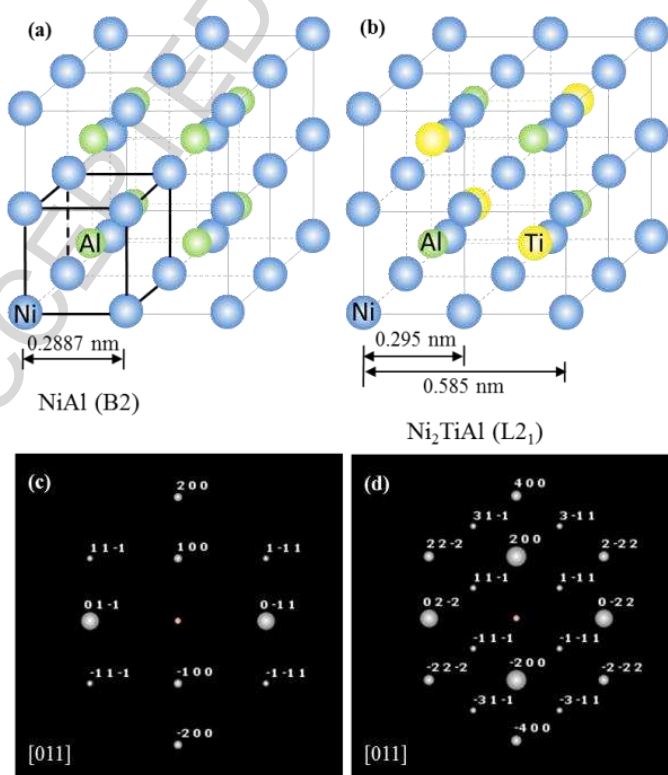

Figure 4 (a) Eight unit cells of B2-ordered NiAl for a better comparison with (b) the unit cell of L2$_1$-ordered Ni$_2$TiAl; diffraction patterns along the [011] zone axis of (c) B2-ordered NiAl and (d) L2$_1$-Ni$_2$TiAl simulated using ICDD PDF-4+ software.
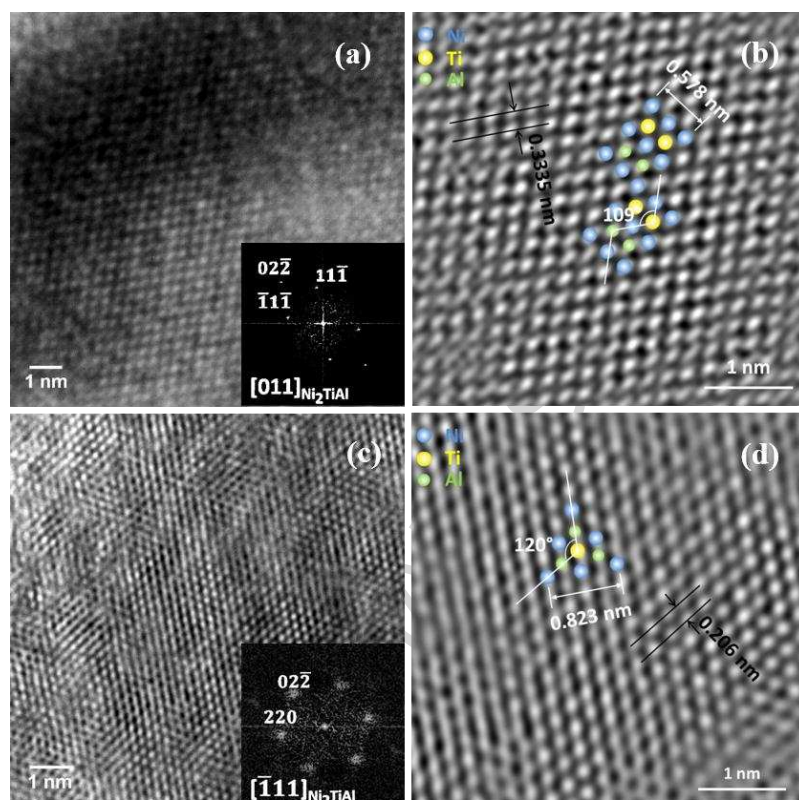
Figure 5 HREM micrographs of precipitates in 12% Mn alloy aged at 500 °C for 10080 min, (a) [011] zone axis; (b) the inversed fast Fourier transform (IFFT) images of (a) by removing the background noise; (c) [$\bar{1}$11] zone axis and (d) IFFT of (c).
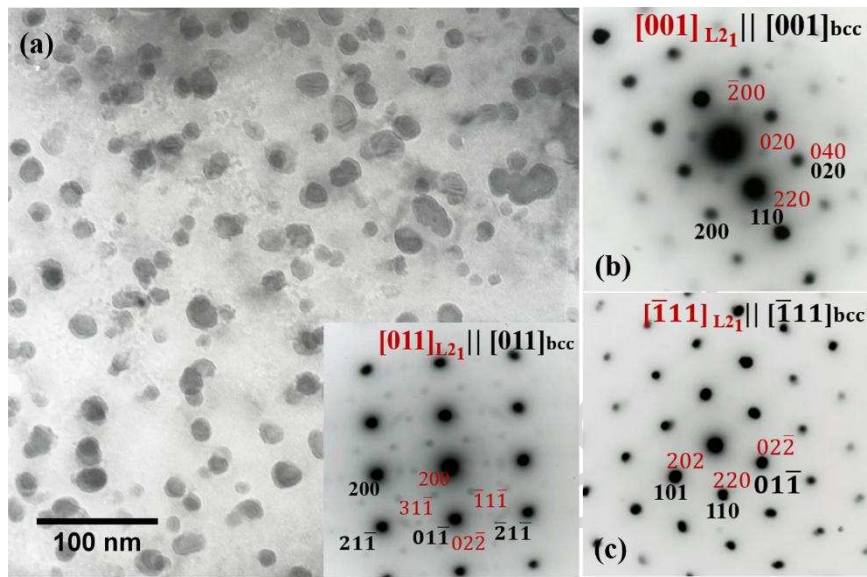
Figure 6 (a) Bright-field micrograph of precipitates and corresponding SAED patterns taken on thin foil sample (500 °C / 10080 min, 10% Mn alloy). SAED patterns obtained along (b) [001] and (c) [$\bar{1}$11] zone axis.
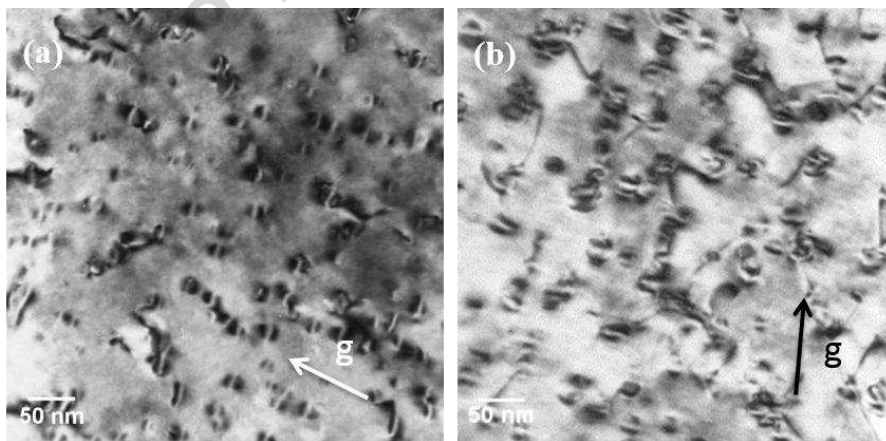

Figure 7 Two-beam bright field TEM micrographs of (a) 7% and (b) 10% Mn alloys after aging at 500 °C for 10080 min. g = <011>
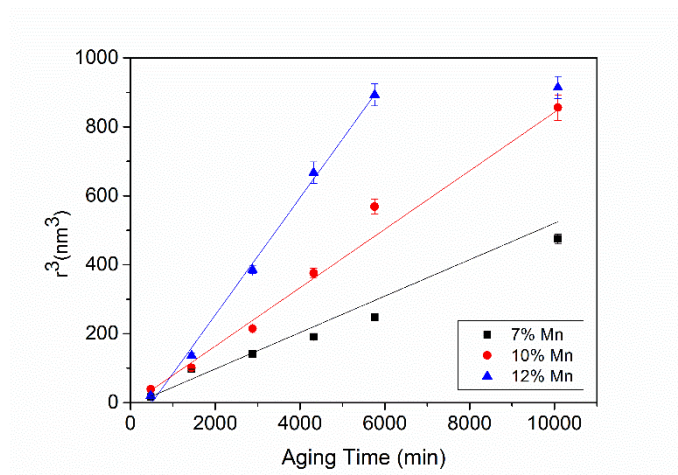
Figure 8 Evolution of the mean precipitate radius $\bar{r}^3$ as a function of aging time t in 7%, 10% and 12% Mn alloys when aging at 500 °C.

Table 1 Chemical compositions (wt.%) of the studied Fe-Mn maraging steels

Alloy	C	Mn	Ni	Mo	Al	Ti	Fe
7% Mn	0.033	7.07	2.03	1.03	1.04	1.05	bal.
10% Mn	0.015	9.97	2.03	1.19	1.00	0.84	bal.
12% Mn	0.022	11.77	1.97	1.17	1.00	0.82	bal.

Characterisation of L2$_1$-ordered Ni$_2$TiAl precipitates in Fe-Mn maraging steels

Highlights

- ➢ Precipitates were identified as L2$_1$-ordered Ni$_2$TiAl for the first time.
- ➢ The L2$_1$-ordered Ni$_2$TiAl phase is coherent and coplanar with the martensite matrix.
- ➢ The precipitates remained coherent with the matrix after long-term aging.
- ➢ An increase in the Mn content of the alloy led to faster precipitation hardening.